A comprehensive structural and magnetic study of Ni nanoparticles prepared by the borohydride reduction of NiCl2 solution of different concentrations

Aparna Roy, V. Srinivas, S. Ram, J. A. De Toro, and J. P. Goff

Additional information on J. Appl. Phys.

A comprehensive structural and magnetic study of Ni nanoparticles prepared by the borohydride reduction of NiCl₂ solution of different concentrations

Aparna Roy[a)] and V. Srinivas
Department of Physics and Meteorology, Indian Institute of Technology, Kharagpur 721302, India

S. Ram
Materials Science Center, Indian Institute of Technology, Kharagpur 721302, India

J. A. De Toro
Departamento de Fisica Aplicada, Universidad de Castilla-La Mancha, 13071 Ciudad Real, Spain

J. P. Goff
Department of Physics, University of Liverpool, Oliver Lodge Laboratory, Liverpool L69 7ZE, United Kingdom

A comparative study of the structure and magnetic properties of Ni nanoparticles (20–80 nm) prepared by the chemical reduction of NiCl₂ solution of four different concentrations is reported. The concentration of the NiCl₂ solution has a profound influence on the room temperature (300 K) magnetic state of the resulting Ni nanoparticles, even though all four samples show the same x-ray diffraction (XRD) pattern, i.e., have the same crystal structure (tetragonal, as proposed by us). It is found that samples obtained from lower concentration solutions (0.1 and 0.5M) show a linear response with magnetic field while those obtained from higher concentration ones (1 and 2M) have a ferromagnetic component at 300 K. This difference in magnetic behavior has been attributed to the possible presence of fcc (face centered cubic) Ni cores in the particles of higher molarity samples, which therefore leads to strong interparticle dipolar interactions in them. The strong interactions, together with the magnetocrystalline anisotropy of the cores, present a significant barrier to the relaxation of core moments in these samples, giving rise to their blocked state even above 300 K, as evident from the irreversibility in the field cooled (FC) and zero field cooled (ZFC) curves, which starts right from the measuring temperature of 390 K. Intriguing features in the form of a sharp peak at 20 K and a hump at 12 K are observed in the ZFC curve of all samples, signaling magnetic transitions at these temperatures. Appreciably high magnetization values are also seen in the *M-H* plots at 5 K. The presence of these low temperature features irrespective of sample molarity indicates that the low temperature magnetic states of the samples, in contrast to their room temperature states, are independent of the concentration of the NiCl₂ solution. © *2006 American Institute of Physics*. [DOI: 10.1063/1.2361013]

I. INTRODUCTION

The synthesis and study of magnetic nanoparticles (NPs) has received considerable attention in the last two decades due to their unusual physical properties and potential applications in catalysts, ferrofluids, and magnetic memory systems.[1–5] A number of physical and chemical methods have been used for the preparation of magnetic nanoparticles. However, chemical methods have the distinct advantage of producing the material in the form of powders, which is the most important requirement in applications such as ferrofluids. Several chemical techniques such as organometallic decomposition, polyol process, and the aerosol and the chemical reduction methods have been used for producing magnetic nanopowders. However, the inherent complexity of the former three methods forbids their widespread use. "Chemical reduction" has thus become an indispensable technique for the production of ultrafine particles of ferromagnetic transition metals, viz., Fe, Co, Ni, and their alloys in powdered form.[6–8] Schlesinger and Brown[9] first reported that transition metal-boron powders can be produced by reduction of the transition metal salt in aqueous solution using an alkali metal borohydride (NaBH₄ or KBH₄). Unfortunately the chemical details of this process are not well understood. Extensive and intensive studies over the last two decades have revealed that variation in reaction conditions or mixing procedures can lead to products of varying nature and composition, variable yields, and many complications that are yet to be understood. An uncertainty thus remains regarding the end product of this reaction.

Past investigations by different groups on the effect of different reaction media and environments on the borohydride reduction of a nickel salt (NiCl₂) revealed that the reaction mechanism differs markedly in aqueous and nonaqueous media and the end product is very sensitive to environmental conditions. However, no consensus could be

a)Electronic mail: aparna@phy.iitkgp.ernet.in

100, 094307-1

reached regarding the compositional identity or the structure of the end product obtained even under similar reaction conditions. For example, Glavee *et al.*[10] reported the formation of Ni and NiO when the reaction is carried out in aqueous medium and in air (i.e., not under inert atmosphere), while Legrand *et al.*[11] after performing x-ray photoelectron spectroscopy (XPS) studies of their samples reported that a mixture of Ni metal and Ni–B is formed under identical conditions. Recently, by investigating the thermal and magnetic behaviors of fine Ni particles prepared by this method, some of us[12] identified the end product to be oxygen-stabilized Ni, i.e., nickel in a tetragonal crystal structure stabilized by the incorporation of oxygen atoms in the Ni lattice. The reaction was performed using aqueous solutions of $1M$ $NaBH_4$ and $1M$ $NiCl_2$, with the dropwise addition of the former to the latter. These investigations revealed that if the reaction is carried out in aqueous medium, in air, at room temperature/ice temperature (i.e., if the precipitate is not exposed to high temperatures) and if the time of addition of $NaBH_4$ is long enough (~ 1 h), boron content of the sample is not significant.

As our previously reported structural analysis[12] is based on Ni nanoparticles prepared using $NiCl_2$ solution of only a single concentration ($1M$), we believe that concentration dependent studies are essential to confirm, without ambiguity, the proposed structural model. In addition, magnetic investigations on the resulting NPs produced from different concentrations of $NiCl_2$ solution would not only be useful for understanding the stability of the new tetragonal phase, but also for filling the void caused by the lack of any systematic study of magnetic properties of fine Ni particles produced by the borohydride reduction method. In this paper we report our comprehensive investigations on the structure and magnetic properties of Ni NPs produced by the borohydride reduction of $NiCl_2$ solution, with concentration varying in the range of $0.1-2M$. The results of only as-prepared samples are discussed. It is found that though the structure of all four samples remains the same, the room temperature (300 K) magnetic properties undergo a striking change—from a paramagnetic state in the case of 0.1 and $0.5M$ samples to the appearance of a significant ferromagnetic component in the 1 and $2M$ samples. The results have been explained with the help of field cooled (FC) and zero field cooled (ZFC) data in conjunction with x-ray diffractograms.

II. EXPERIMENTAL DETAILS

Fine particles of Ni were prepared by reducing the nickel salt $NiCl_2 \cdot 6H_2O$ with sodium borohydride ($NaBH_4$) as reducing agent. The reaction was carried out in aqueous medium, at room temperature and ambient atmosphere. 200 ml of a $1M$ solution of $NaBH_4$ was added dropwise over a period of 1 h to 500 ml of a $0.1M$ $NiCl_2 \cdot 6H_2O$ solution in a beaker, with constant magnetic stirring. The reaction was repeated for three more concentrations of $NiCl_2$ solution (0.5, 1, and $2M$), with the reductor molarity kept fixed at $1M$. The details of the sample preparation and the proposed reaction mechanism can be found in Ref. 12.

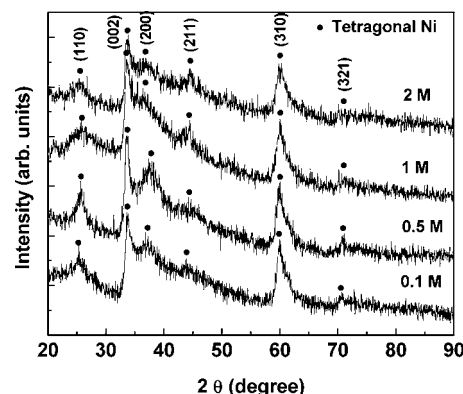The crystalline structure of the samples was studied by

FIG. 1. X-ray diffractograms of samples prepared from $NiCl_2$ solutions of different molar concentrations. The Miller indices of the peaks of tetragonal Ni are also marked.

x-ray diffraction (XRD) using a Philips PW 1718 x-ray diffractometer with filtered Cu $K\alpha$ radiation of wavelength $\lambda = 0.154\,18$ nm. The microstructure was studied with a JEM 2000cx transmission electron microscope (TEM). The thermal stability [differential thermal analysis (DTA)/thermogravimetric analysis (TGA)] of the sample was studied using a Perkin Elmer Instruments thermogravimetric/differential thermal analyzer, in the temperature range of $375-1080$ K, with a heating rate of 10 K/min and in a flow of argon gas at 100 ml/min.

The room temperature (300 K) *M-H* [magnetization (*M*) versus field (*H*)] curves were measured with a vibrating sample magnetometer using magnetic fields up to 14 kOe. The FC/ZFC curves and the *M-H* curves at 5 K were measured with a superconducting quantum interference device (SQUID) magnetometer (Quantum Design).

III. RESULTS AND DISCUSSION

A. Structure and phase stability

The x-ray diffractograms of the samples prepared using the four mentioned concentrations of $NiCl_2$ solution are shown in Fig. 1. A crystalline structure with some degree of disorder/amorphosity possibly stemming from surface layers is evident from the patterns. No oxide peaks are observed which suggest that the oxides, if present in the particles, are in the amorphous phase or nonstoichiometric. Similar diffraction patterns[10] have been observed even when millimolar concentration of $NiCl_2$ is used. The diffraction patterns neither correspond to face centered cubic (fcc) Ni nor to NiO. However, as discussed recently in our previous work,[12] we have indexed the peaks of these diffractograms assuming a tetragonal crystal structure with space group $14/mcm$. We have proposed that a tetragonal Ni lattice gets derived from the fcc Ni lattice by the incorporation of oxygen atoms at the interstitial positions of the latter, forming a solid solution of Ni and oxygen. Presence of this dissolved oxygen in the sample modifies the usual fcc crystal structure of the Ni particles, straining and hence making them tetragonal.

The Miller indices corresponding to each peak in the diffraction pattern of tetragonal Ni are marked in Fig. 1. Table I shows the lattice parameters *a* and *c* for all four

TABLE I. Variation of lattice parameters a and c with $NiCl_2$ concentration.

Sample	Lattice parameter (Å)		Unit cell volume (Å)^3	c/a
	a	c		
0.1M	4.920	5.355	129.62	1.088
0.5M	4.912	5.342	128.89	1.087
1.0M	4.905	5.330	128.23	1.086
2.0M	4.890	5.322	127.26	1.088

FIG. 3. DTA and TGA profiles of the 1M sample obtained with a heating rate of 10 K/min in argon atmosphere.

as-prepared samples. There is a small but significant decrease of both a and c with increase in molarity of the $NiCl_2$ solution. Although the c/a ratio is observed to be almost constant, the volume of the unit cell decreases as the concentration is increased. Since the volume of a unit cell in fcc Ni is much smaller than the corresponding volume in tetragonal Ni, the decrease in volume with increase in concentration may be attributed to the growth of fcc phase at higher concentrations. The same phenomenon, namely, the growth of fcc phase and the subsequent reduction in cell volume, was also observed on annealing the as-prepared sample in air.[13]

The XRD patterns of one of the samples (1M) annealed in H_2 gas at 573 and 773 K are presented in Fig. 2(a). The 573 K annealed sample clearly shows the simultaneous existence of both fcc Ni and tetragonal Ni while that annealed at 773 K shows peaks of only pure fcc Ni. The same features have been observed in the diffraction patterns of the remaining three samples. Figure 2(b) shows the XRD patterns of all four samples annealed in H_2 at 773 K. Very similar diffractograms with no trace of elemental boron or its compounds were obtained on annealing the samples at 973 K in argon.[13] The observation of peaks of only fcc Ni in these samples suggests that impurities in the form of boron or its derivatives, even if present, are in an insignificant amount. The
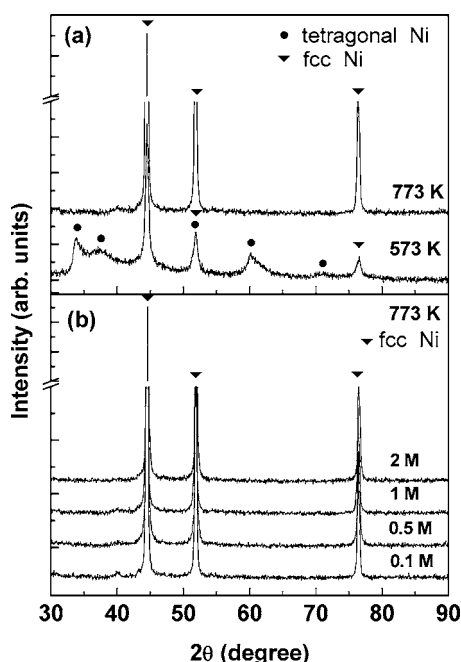
only element, besides Ni, that is present substantially in the as-prepared powder is oxygen. Removal of this dissolved oxygen from the Ni lattice results in the return of Ni back to its usual fcc structure. Furthermore, the complete absence of any NiO peak in the XRD patterns of samples annealed in H_2 [Fig. 2(b)] or inert atmosphere (argon, not shown) suggests that even if some nonstoichiometric and Ni-defective oxides are present in as-prepared samples, they are unstable.

In order to investigate further the structure and phase stability of the as-prepared samples, thermal analysis experiments have been performed under argon atmosphere. We have studied the thermal evolution of the phases by both DTA and TGA techniques. The DTA and TGA profiles of the 1M sample are shown in Fig. 3. An endothermic peak at 655 K separating two exothermic peaks at 551 and 713 K is observed in the profile. The broad exothermic peak at 551 K is probably due to the crystallization of any amorphous species (possibly NiO, because the samples have been prepared in ambient atmosphere and hence surface passivation by a thin layer of nickel oxide—stoichiometric/non-stoichiometric/Ni defective—is inevitable) present in the surface layers while the endothermic peak at 655 K appears to be due to the desorption of the dissolved oxygen from the tetragonal lattice. This triggers the collapse of the tetragonal structure of the Ni nanoparticles and the subsequent evolution of the fcc phase. The sharp exothermic peak at 713 K signals the release of strain energy and the transformation to the fcc phase. The TGA curve shows a steep fall with a 15.6% weight loss in the sample at 713 K. Assuming the complete weight loss to be due to the desorption of interstitial oxygen from the Ni lattice, the atomic composition of the 1M sample has been calculated to be $Ni_{60}O_{40}$. Likewise, the TGA profile of the 0.1M sample[13] shows a weight loss of 19% from which the atomic composition of the sample is found to be $Ni_{54}O_{46}$. A sample prepared from a lower molarity $NiCl_2$ solution thus has higher oxygen content.

Figures 4(a) and 4(b) are respectively the TEM micrographs of the 1 and 2M samples with spherical particles of average diameters of 65 and 80 nm. Figures 4(c) and 4(d) show the electron diffractograms of the 0.5 and 1M samples, respectively. A broad halo along with few indistinct rings is observed in the diffractograms. The halo is reminiscent of the amorphous content of the samples, whereas the rings

FIG. 2. X-ray diffraction patterns of (a) 1M sample annealed in H_2 gas at 573 and 773 K and (b) all four samples annealed in H_2 gas at 773 K.
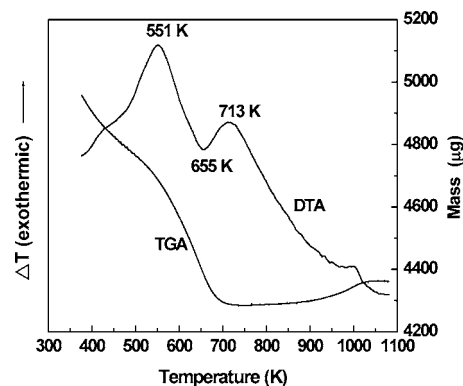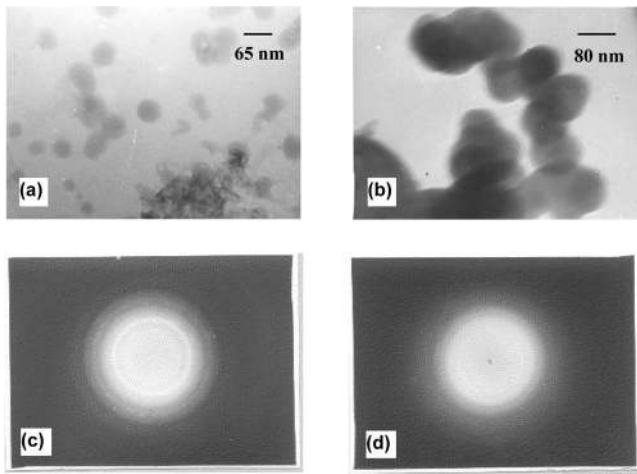
FIG. 4. TEM micrographs of (a) 1*M* and (b) 2*M* samples showing spherical particles of diameter 65 and 80 nm, respectively. (c) and (d) are the electron diffractograms of the 0.5 and 1*M* samples, respectively.

typify the crystalline part. The electron diffractograms thus depict the sample to be partly disordered and partly crystalline in close agreement with x-ray diffraction results.

B. Magnetic properties

A preliminary assessment of the magnetic state of the samples has been done through their magnetization (M) versus field (H) plots at 300 K. Figure 5 shows these plots for the four samples prepared from the specified concentrations of $NiCl_2$ solution. Several interesting features can be noted from this figure: (i) low magnetization values compared to fcc Ni for all samples even at an applied field as high as 10 kOe, (ii) a linear magnetization response with applied field for the lower concentration (0.1 and 0.5*M*) samples, (iii) hysteretic magnetization for higher concentration (1 and 2*M*) samples with a sharp increase in magnetization at low fields followed by a linear nonsaturating behavior, and (iv) increased values of magnetization (M), remnant magnetiza-
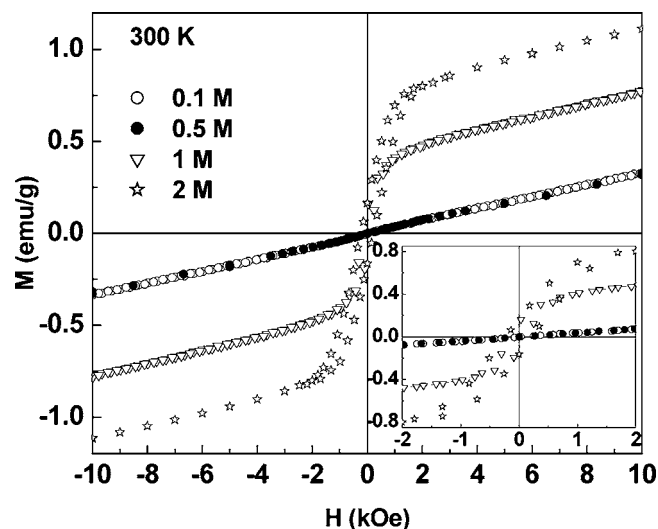

FIG. 5. *M-H* plots at 300 K, for 0.1, 0.5, 1, and 2*M* samples. Inset: an expanded view of the plots clearly showing hysteresis in the case of 1 and 2*M* samples.

tion (M_r), and coercivity (H_c) in case of 2*M* sample as compared to the 1*M* sample (see inset). In the following sections we give plausible explanations of the above features.

1. Low magnetization values of the samples

The magnetization values of all four samples are significantly lower than that of pure fcc Ni. A first inspection would make one attribute this to the change of size from bulk to nanoregime. However, it has been shown[14] without ambiguity that pure fcc Ni even when nanosized does not show any significant change in its saturation magnetization, though impurities can bring down the magnetization value quite significantly. Since the samples have been prepared in ambient atmosphere, oxygen contamination can be expected to play a major role in the reduction of magnetization values. The proposed tetragonal crystal structure of Ni (Ref. 12) stabilized by an interstitially dissolved oxygen atom in the (002) plane hints at these dissolved oxygen atoms modifying the magnetic properties substantially. This has been discussed at length in one of our recent works,[13] where we have attributed an antiferromagnetic superexchange interaction between some of the Ni atoms, mediated by the dissolved oxygen atoms in the Ni lattice, to eliminate Ni ferromagnetism and give rise to a paramagnetic state in the oxygen-stabilized (OS) tetragonal phase of Ni. The magnetization response of the as-prepared samples (with applied field) therefore, quite expectedly, shows low values typical of a paramagnet, since all four samples have paramagnetic OS tetragonal Ni as the majority phase constituting their particles.

2. Linear nonhysteretic response with field for 0.1 and 0.5M samples

In spite of being constituted primarily of OS tetragonal Ni, a difference is observed in the magnetic state of the lower (0.1 and 0.5*M*) and higher molarity (1 and 2*M*) samples, with the former being paramagnetic at room temperature and the latter exhibiting a clear ferromagnetic component. This can be rationalized in terms of the possible presence of fcc Ni cores in the particles of the latter sample, as described in Sec. III B 3. The fcc cores are absent in the former set of samples since their (samples) low Ni content resulting from the low molarity of the $NiCl_2$ solution does not lead to the formation of Ni fcc cores in them. Hence the samples exhibit a linear magnetization response with applied field with susceptibility $dM/dH = 2.5 \times 10^{-5}$ emu/g Oe (as obtained from Fig. 5), typical of a strong paramagnet. The FC/ZFC curves shown in Fig. 6(a) with complete reversibility in the temperature range of 70–200 K further confirm the paramagnetic state of these powders. However, the small deviation from reversibility below 70 K indicated by the faint bifurcation of these curves at this temperature may be due to the blocking of a few relatively large particles supporting a minority fcc phase, given the unavoidable distribution of particle sizes.

3. Magnetic states of 1 and 2M samples

Three key features need to be addressed regarding the magnetic state of the 1 and 2*M* samples at room temperature.
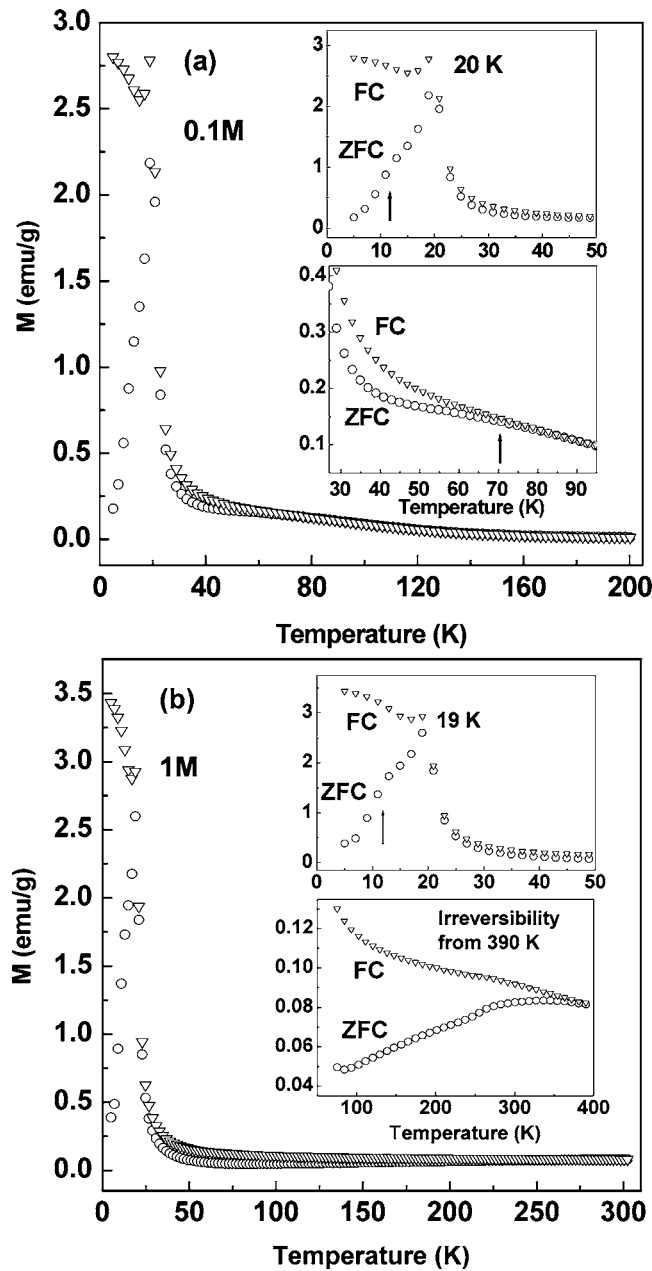
FIG. 6. (a) Magnetization of FC and ZFC particles of 0.1*M* sample, in 100 Oe applied field, as a function of temperature. Insets: expanded views of the *M-T* plot for two different temperature regimes of 0–50 and 30–90 K. The latter clearly shows the bifurcation of the FC and ZFC curves at ~70 K, hinting at the blocked state of the particles below this temperature. The curves, however, remerge at 22 K and separate again at 20 K, indicating a transition to some other state. (b) *M-T* plot of 1*M* sample. Inset: expanded view of the plot for the temperature regimes of 0–50 and 50–400 K. The former indicates that the transition at 20 K is present in this sample too. The latter shows the irreversibility between FC and ZFC curves right from the measuring temperature, indicating the blocked state of the particles at 300 K.

(i) Origin of the ferromagnetic contribution to the magnetic signal.

(ii) Origin of the linear component in their net magnetization.

(iii) Increased values of magnetization, coercivity and remnant magnetization of the 2*M* sample as compared to 1*M* sample.
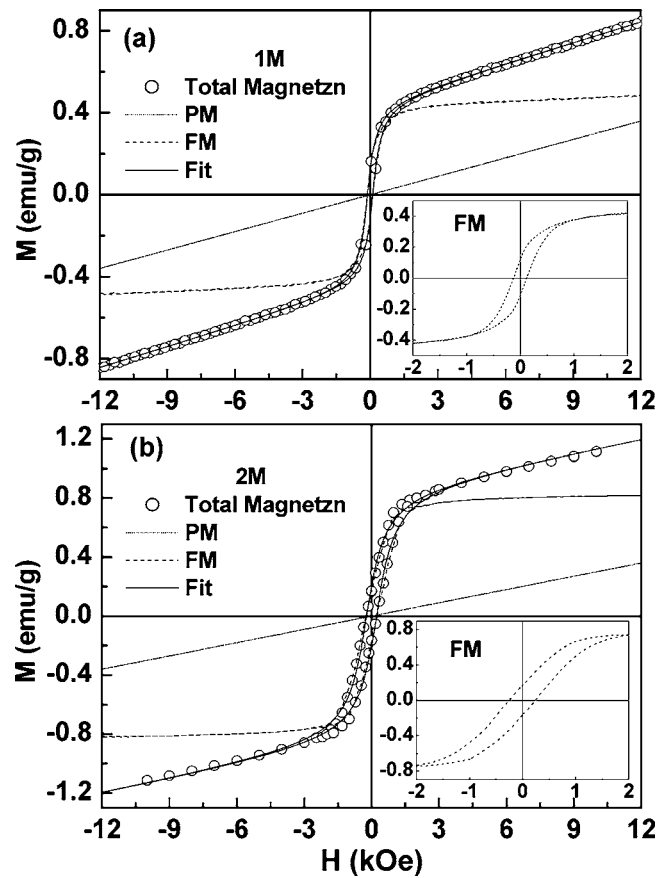

FIG. 7. (a) Total magnetization (*M*) as a function of applied field (*H*) at 300 K for the 1*M* sample, with its paramagnetic (PM) and ferromagnetic (FM) components separated. The bold line represents the fit of Eq. (1) to the total magnetization. Inset: an expanded view of the FM component. (b) Plot of above features for the 2*M* sample.

In order to have a clear understanding of the above features, the magnetization curves at 300 K of the 1 and 2*M* samples were fitted to the following expression[15] comprising a ferromagnetic (FM) and a paramagnetic (PM) part:

$$M(H) = \frac{2M_S}{\pi} \tan^{-1}\left[\frac{H \pm H_C}{H_C} \tan\left(\frac{\pi S}{2} \right) \right] + \chi H. \tag{1}$$

The first term is the usual function customarily used to fit FM hysteresis curves while the second term accounts for the PM component with χ as the magnetic susceptibility. The quantities M_S and H_C give, respectively, the saturation magnetization of the FM part and coercivity of the hysteresis loop. S is known as "squareness" of the FM loop and is defined as the ratio of remanent magnetization to saturation magnetization of the FM component, i.e., $S = M_R/M_S$. Reasonably good fits to the magnetization curves have been obtained for both samples. These are shown in Figs. 7(a) and 7(b) along with the separated components. Table II compares the magnitude of M_R, H_C, M_S, and χ for both samples as obtained from the fits.

To extract some meaningful information from the fitting parameters, the PM component of the 1 and 2*M* samples and the *M-H* data (at 300 K) of the 0.1 and 0.5*M* samples have been plotted in the same graph (Fig. 8). Interestingly enough, all four plots merge, indicating that the PM component in the

TABLE II. Magnitude of the fitting parameters M_R, H_C, M_S, and χ for 1 and 2M samples.

Sample	M_S (emu/g)	M_R (emu/g)	H_C (Oe)	χ (emu/g Oe)
1M	0.4535	0.121	126.26	0.000 03
2M	0.8650	0.208	236.21	0.000 03

former samples is of the same magnitude as the total magnetization of the latter ones. The origin of the linear nonhysteretic response of the lower molarity samples (particles constituted only of tetragonal Ni) and the PM component of the higher molarity ones thus essentially appears to be the same. A convincing explanation of the FM component in the 1 and 2M samples then requires the existence of a small fcc Ni core[16] in the particles, in addition to the usual tetragonal part. Each particle in the 1 and 2M samples has, therefore, a dominant tetragonal Ni (*t*-Ni) part and possibly a small fcc Ni core, with the net magnetic moment of a particle at moderate fields coming mostly from the fcc Ni cores. On the other hand, the nonsaturating PM component in the net magnetization of the 1 and 2M samples can clearly be attributed, as commented above, to the *t*-Ni part of the particles as evident from an inspection of Fig. 8.

In both 1 and 2M samples, the higher molarity of the NiCl$_2$ solution produced particles with higher Ni content and much bigger size (65 and 80 nm for the 1 and 2M samples, respectively). Similar results have also been reported by Chinnasamy *et al.*,[17] in the case of *hcp* (hexagonal close packed) Ni nanoparticles prepared by the reduction of nickel acetate tetrahydrate using a polyol [tetraethylene glycol (TEG) or trimethylene glycol (TMEG)]. The authors observed an increase in particle size for samples prepared from solutions having higher Ni ion concentration. This profusion of Ni atoms might be one of the reasons for the development of the fcc Ni region, though we are yet to fully comprehend it. We propose that the hysteretic response of the 1 and 2M samples is a manifestation of the blocked state of the ferromagnetically ordered fcc Ni cores in their particles. The FC/ZFC curves in the inset of Fig. 6(b) confirm this state through the irreversibility in the curves, which starts right

FIG. 8. Total magnetization (M) as a function of applied field (H) at 300 K for ($\bigcirc$) 0.1M and ($\triangle$) 0.5M samples. ($\star$) and ($\square$) represent, respectively, the paramagnetic components for 1 and 2M samples, obtained from the fit of Eq. (1) to their total magnetization.

from the measuring temperature of 390 K. A pertinent question, which needs to be addressed at this point, is the cause of the blocked state of the cores. It is well known that blocking of magnetic nanoparticles at a temperature T is determined by two main factors: (i) particle size, involving the idea that the particle will be stable when the thermal energy k_BT at the temperature of the experiment is less than the energy barrier KV posed by the magnetocrystalline anisotropy (K is anisotropy constant and V is particle volume) and (ii) interparticle interactions (in moderately concentrated dispersions, mainly of the dipolar type), which effectively increase the energy barrier to moment relaxation (and thus the blocking temperature) or even give rise to a collective state where the blocking (now freezing) temperature depends on the strength of the interactions.

Considering the blocked state of the fcc Ni cores to be solely due to their size [possibility (i)], a rough estimate of the core size was obtained (ignoring contribution from surface anisotropy) from the equation

$$K_1 V = 25.33 \times k_B T_B, \qquad (2)$$

where K_1 is the first order magnetocrystalline anisotropy constant of bulk fcc Ni, V is the volume of the cores, T_B is their blocking temperature, and k_B is the Boltzmann constant. With $K_1 = 0.5 \times 10^4$ J/m^3 and $T_B = 390$ K, the diameter of the fcc cores has been estimated to be 37.3 nm. This big size, however, seems quite impractical, considering the presence of only very moderate fcc Ni reflections in the XRD patterns of the higher molarity samples and also the nonobservation of any large magnetization in their *M-H* plots at room temperature, which (large magnetization) is expected if such a significant Ni-rich fraction constitutes the particles of these samples. We therefore conclude that the fcc Ni cores in the particles of the higher molarity samples are rather small, quite smaller than the critical size of 19 nm (Ref. 18), below which they exist as single domains. However, strong interactions between these cores, coupled with their magnetocrystalline anisotropy, lead to a significant energy barrier to their moment relaxation, giving rise to their blocked state even at 390 K.

The increased values of M_R, H_C, and M_S in the 2M sample can be explained on the basis of the larger particle size (80 nm) of this sample in comparison with the 1M sample (65 nm). This might lead to slightly larger dimensions of the fcc Ni core in the particle and hence to a larger moment which in turn can give rise to stronger interactions between 2M particles. Hence, once aligned in the field direction, it is more difficult in the case of the 2M particles to revert their moment directions with reversal of field, as compared to the 1M particles. Substantial amount of M_R thus remains and higher coercive field is required to bring back the magnetization to zero. The larger size of the fcc core implying an increase in the Ni-rich volume fraction in the 2M sample, also justifies the higher M_S value observed in this sample.
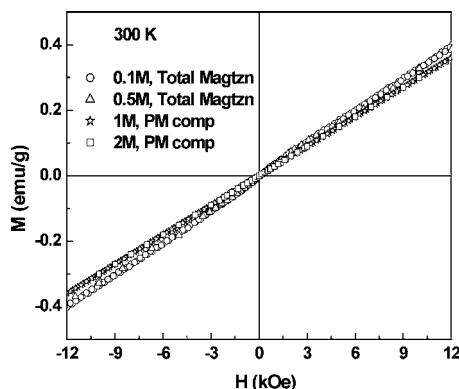
4. Low temperature magnetic states: Effect of concentration

From Fig. 5 it is seen that the variation of concentration of the $NiCl_2$ solution has induced profound changes in the room temperature magnetic state of the as-prepared samples. It is then important to check whether the low temperature magnetic state of these samples is dependent on or independent of the molarity of the $NiCl_2$ solution. This information can be obtained by tracing out the thermal variation of magnetization i.e., M-T curves of the samples. Figure 6 shows these curves for one low concentration ($0.1M$) and one high concentration ($1M$) sample, measured in zero field cooling and field cooling conditions under an applied field of 100 Oe from 200 K to 5 K and 390 K to 5 K, respectively. Strong irreversibility in the FC/ZFC curves below 20 K with a very sharp and well-defined peak in the ZFC curve at this temperature, indicative of a phase transition, is observed for both samples. Furthermore, a small hump at ~12 K is also seen in the ZFC magnetization curve of both samples, implying yet another magnetic transition.

Thus although concentration variation of $NiCl_2$ solution induces changes in the room temperature magnetic state of the samples, their low temperature states are surprisingly independent of concentration. However, not much can be said about the nature of the low temperature transitions since the bifurcation in FC/ZFC curves is a typical signature of the metastable nature of the magnetization and is exhibited by various magnetically disordered systems such as spin glasses, cluster glasses, superparamagnets, and even inhomogeneous ferromagnets. Hence rigorous ac susceptibility (ACS) measurements are needed before metastability at 20 and 12 K is attributed to any of the above-mentioned causes. These are presently in progress and are the subject of our future publication.

It is interesting to point out here that the presence of a PM component in the M-H plots at 300 K and the peak at 20 K in FC/ZFC curves appear in all four samples prepared from the specified concentrations of $NiCl_2$ solution. Furthermore, the tetragonal phase of Ni exists as a major component in all these samples. This makes us believe that it is the tetragonal phase of Ni which gives rise to the above features (PM component and 20 K peak) because of the relatively high oxygen concentration in this phase. The M-H plot of the $1M$ sample at 5 K (Fig. 9) showing inordinately high values of magnetization as compared to that at 300 K (other samples also show similar behavior) seems to provide some clue about the nature of the transition at 20 K. Probably the oxygen-stabilized tetragonal Ni phase of the particles undergoes transition from its room temperature paramagnetic state to a ferromagnetic state at 20 K, imparting large magnetic moment to the particles. On application of a magnetic field at 5 K these macromoments align in the field direction leading to the large magnetization enhancement at this temperature.

A second reason for the high magnetization values might be the low boron content in our sample. This rules out the possibility of use up of Ni for the formation of any paramagnetic borides—stoichiometric or nonstoichiometric—and keeps the sample relatively high in Ni content. We mention here in passing that such high magnetization values at low
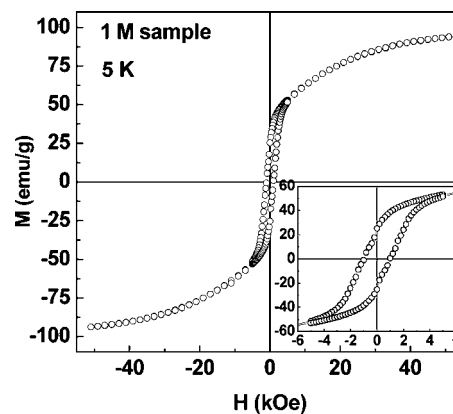

FIG. 9. M-H plot at 5 K for the $1M$ sample. Inset: an expanded view of the plot.

temperatures (5, 15, and 20 K) have also been reported by De Biasi *et al.* in Fe–Ni–B (Ref. 19) and Co–Ni–B (Ref. 20) nanoparticles prepared by the borohydride reduction method. According to their observations, the effect is very much pronounced in diluted dispersions of the samples (interparticle distance ~35 and 16 nm for Fe–Ni–B and Co–Ni–B particles, respectively), in comparison to undispersed samples in which particles are in contact. They have attributed the high magnetization values to the formation of ferromagnetic clusters of spins at the particle surface, which (clusters) readily align in the field direction on application of magnetic field. In the undispersed sample, because of the presence of strong interparticle interactions, ferromagnetic cluster formation is frustrated and magnetization does not increase as strongly at low temperature. This explanation is, however, inappropriate in the case of our samples since these are totally undispersed (hence have strong interparticle interactions) and yet show very high magnetization values at 5 K.

IV. CONCLUSION

The structure and magnetic properties of fine Ni nanoparticles prepared by the chemical reduction of $NiCl_2$ solution of four different concentrations (in the range of $0.1-2M$) have been investigated. From these investigations we arrive at the following conclusions. (i) The x-ray diffraction patterns and phase stability studies (DTA/TGA) indicate that Ni is stabilized in a tetragonal crystal structure, different from its usual fcc structure, due to the presence of interstitial oxygen atoms. This tetragonal phase of Ni is the dominant component in both high and low molar concentration samples. (ii) The lower concentration samples show PM behavior at room temperature while the higher concentration ones show a superposed FM component along with a PM component. The PM component of all samples stems from the tetragonal phase of Ni (majority phase), where the oxygen in solid solution eliminates Ni ferromagnetism at room temperature. (iii) The significant room temperature ferromagnetic component of the higher molarity samples arises from single-domain particles with a blocking temperature higher than 390 K. This, along with the reduction of unit cell volume in these samples, may be indicative of the possible presence of fcc Ni core in them. (iv) The magnetic phase

transitions reflected by the peak at 20 K and the hump at 12 K in the ZFC curve is observed in samples prepared from both higher and lower molarity $NiCl_2$ solutions. Thus the low temperature magnetic states are independent of the concentration of $NiCl_2$ solution in contrast to the room temperature states. (v) The high magnetization values in the *M-H* plots at 5 K is probably due to the oxygen-stabilized tetragonal Ni phase of the particles undergoing transition from its room temperature paramagnetic state to a ferromagnetic state at 20 K.

ACKNOWLEDGMENT

[1] J. L. Dormann, D. Fiorani, and E. Tronc, Adv. Chem. Phys. **98**, 283 (1997).

[2] J. L. Dormann and D. Fiorani, in *Magnetic Properties of Fine Particles*, edited by J. L. Dormann and D. Fiorani (North-Holland, Amsterdam, 1992).

[3] J. D. Hood, M. Bedranski, R. Frausto, S. Guccione, R. A. Reisfeld, R. Xiang, and D. A. Caresh, Science **296**, 2407 (2002).

[4] P. Tartaj, M. P. Morales, S. V. Verdaguer, T. G. Carreno, and C. J. Serna, J. Phys. D **36**, R182 (2003).

[5] J. M. Nam, C. S. Thaxton, and C. A. Mirkin, Science **301**, 1884 (2003).

[6] I. Lisiecki and M. P. Pileni, J. Am. Chem. Soc. **115**, 3887 (1993).

[7] S. H. Wu and D. H. Chen, J. Colloid Interface Sci. **259**, 282 (2003).

[8] S. Wei, H. Oyanagi, Z. Li, X. Zhang, W. Liu, S. Yin, and X. Wang, Phys. Rev. B **63**, 224201 (2001).

[9] H. I. Schlesinger and H. C. Brown, J. Am. Chem. Soc. **75**, 215 (1953).

[10] G. N. Glavee, K. J. Klabunde, C. M. Sorensen, and G. C. Hadjipanayis, Langmuir **10**, 4726 (1994).

[11] J. Legrand, A. Taleb, S. Gota, M. J. Guittet, and C. Petit, Langmuir **18**, 4131 (2002).

[12] A. Roy, V. Srinivas, S. Ram, J. A. De Toro, and J. M. Riveiro, J. Appl. Phys. **96**, 6782 (2004).

[13] A. Roy, V. Srinivas, S. Ram, J. A. De Toro, and U. Mizutani, Phys. Rev. B **71**, 184443 (2005).

[14] H. Kisker, T. Gessmann, R. Wurschum, H. Kronmuller, and H. E. Schaefer, Nanostruct. Mater. **6**, 925 (1995).

[15] M. B. Stearns and Y. Cheng, J. Appl. Phys. **75**, 6894 (1994).

[16] A possibility seems to exist for this fcc core. From XRD patterns (Fig. 1) it is seen that the peak near $2\theta = 44.5°$ becomes more intense with increasing molar concentration, suggesting the growth of more and more planes of the related (*hkl*) indices. This peak corresponds to the (211) plane of tetragonal Ni (Ref. 12) and has a normalized intensity of 52. However, the same peak is the most intense peak of fcc Ni and appears due to reflection from (111) planes. Therefore, possibly with increasing molar concentration, a faint fcc region develops in each particle, though the tetragonal part is absolutely dominant.

[17] C. N. Chinnasamy, B. Jeyadevan, K. Shinoda, K. Tohji, A. Narayanasamy, K. Sato, and S. Hisano, J. Appl. Phys. **97**, 10J309 (2005).

[18] D Jiles, *Introduction to Magnetism and Magnetic Materials* (Chapman & Hall, 1991), p. 410.

[19] E. De Biasi, C. Ramos, R. D. Zysler, and H. Romero, Phys. Rev. B **65**, 144416 (2002).

[20] R. D. Zysler, H. Romero, C. A. Ramos, E. De Biasi, and D. Fiorani, J. Magn. Magn. Mater. **266**, 233 (2003).